Int. J. Solids Structures Vol. 29, No. 21, pp. 2623–2638, 1992
Printed in Great Britain.

0020-7683/92 $5.00 + .00

SELF-CONSISTENT CONSTITUTIVE MODELING AND TESTING OF POLYCRYSTALLINE HASTELLOY-X

SHIXIANG SHI and ERIC H. JORDAN
University of Connecticut, Storrs, CT 06268, U.S.A.

and

KEVIN P. WALKER
Engineering Science Software Inc., Smithfield, RI 02917, U.S.A.

(*Received* 16 *December* 1991; *in revised form* 3 *March* 1992)

Abstract—A viscoplastic constitutive model is presented for the estimation of the overall mechanical response of Hastelloy-X polycrystalline metal from a knowledge of the single crystal behavior. The deformation behavior of the polycrystal is derived from that of single crystals by using a self-consistent method. The single crystal behavior is developed by summing postulated slip on crystallographic slip systems. Plasticity and creep are modeled using a unified viscoplastic model which includes the interaction effects between rapid and slow deformation at elevated temperature. The validity of the model is directly tested by critical experiments on Hastelloy-X in both the single crystal and polycrystalline versions.

1. INTRODUCTION

Real polycrystalline metals consist of large numbers of randomly orientated single crystal grains. Direct modeling of an array of grains large enough to give a representative behavior of the polycrystal is currently infeasible. Such an array would comprise a three-dimensional, inhomogeneous, nonlinear model with many degrees of freedom. Accordingly an idealization must be made and here we use the self-consistent idealization [see, for example, Hutchinson (1976), Berveiller and Zaoui (1984), Kratochvil and Tokuda (1984), Bretheau *et al.* (1984), Chiang and Weng (1984), Duva (1984) and Nemat-Nasser and Obata (1986)]. In this idealization the behavior of a single spherical crystal grain embedded in an effective isotropic medium is found using Eshelby's solution (1957). The properties of the effective medium are derived from averaging the behavior of embedded grains of representative orientations. A unified viscoplastic single crystal formulation (Jordan *et al.*, 1992) is used to describe the behavior of each grain with a representative orientation at elevated temperature. Since the properties of the effective medium depend on the average behavior of the grain, as constrained by the effective medium, the idealization results in implicit equations. However, in the inelastic problem an incremental solution must be used and these incremental equations turn out to be explicit provided an Euler forward difference solution scheme is used. To directly verify the validity of the model, critical experiments were performed on both the single crystal and polycrystalline versions of the same material at elevated temperature. This strategy tests the self-consistent method in a way that is least intertwined with the adequacy of the single crystal model.

The goal of the present work is to predict the viscoplastic behavior of a polycrystalline metal beginning with a formulation at the crystallographic slip level and then to quantitatively test these predictions. The formulation herein is based on a small strain assumption and accordingly no rotational effects in the microstructure are considered. In addition, no provision is made to account for grain boundary sliding effects between the crystalline grains. In order to quantitatively test such a model it is necessary to run tests on both the single crystal and the polycrystal versions of the same alloy and ensure that the single crystal samples have properties which closely match those of the single crystal grains in the polycrystal sample. There are formidable difficulties in running such tests. First, it is necessary to obtain macroscopic single crystal samples and either test several orientations or else test the sample using several different stress states. Second, it is necessary to ensure

that the single crystal specimens have properties which closely match those of the single crystal grains in the polycrystal sample. Finally, it is necessary to construct a suitable constitutive model for the highly anisotropic single crystal and verify its predictions at the single crystal level. Because of these difficulties critical experiments have rarely been performed.

In this investigation large single crystal samples were made using procedures developed for making single crystal turbine blades at Pratt & Whitney. A single orientation [001] set of specimens was made and tested in tension–torsion to obtain information about the anisotropy. The alloy chosen (Hastelloy-X) is a single phase gamma nickel base alloy that is solution strengthened by very fine carbides. The primary determinant of strength is the carbon saturation. Both the single crystal and polycrystal samples were heat treated simultaneously in an attempt to equalize the carbon saturation between the single and polycrystal samples and therefore give them identical properties. The final problem of modeling the anisotropic behavior of the single crystal was solved using a slip based viscoplastic constitutive model in which the anisotropy is predicted from information about the slip geometry. The development and verification of such a model is of sufficient complexity that it has been described in a separate paper (Jordan *et al.*, 1992). Here we will summarize the single crystal model, present the self-consistent polycrystalline model, and show the comparison between the self-consistent model and the polycrystalline experiments to test the theory.

2. CRITICAL EXPERIMENTS

The experimental set-up used in this work has been described elsewhere in detail (Jordan and Chan, 1987). Here we briefly summarize the relevant features. A high ductility, single phase, solution strengthened aircraft engine alloy, Hastelloy-X, was chosen for both the single crystal version and the polycrystalline version because of its simple phase composition, and particularly because of its availability in large single crystal form. This material is a nickel base alloy which has relatively low strength but high ductility at elevated temperatures. The chemical composition of the Hastelloy-X is given in Table 1. Both the single crystal and polycrystalline material were subjected to an identical pretesting heat treatment at a temperature of 1204°C for 1 hr. The specimen geometry used was identical for both the single crystal and the polycrystal. The gage section was a thin walled tube with a mean diameter of 16.5 mm and a wall thickness of 1.27 mm.

All the elevated temperature tests conducted for this work were performed on a computer controlled tension–torsion servo-hydraulic testing machine designed and built at the University of Connecticut (Jordan and Chan, 1987). Axial stress was calculated by dividing the load by the area whilst torsional shear stress was calculated using the formulae for a thin walled tube, assuming a uniform distribution through the wall. Strain was measured using an extensometer which is a variant of that developed by Liu (1983). This extensometer has less than 0.5% cross talk. The samples were heated using an audio frequency induction heater controlled by gage section temperatures measured using an infrared pyrometer. The temperature was further checked using an optical match wire pyrometer with thermocouples welded just outside the gage section.

In both the tests required to develop the single crystal model and the tests to explore the polycrystal properties, a wide range of different test conditions were conducted at 982°C. A fortuitous feature of the material response is the minimal cyclic hardening at this temperature. In addition, the samples showed no persistent deformation history effects in

Table 1. Hastelloy-X chemical composition

Element	C	Cr	Co	Mo	W	Fe	Mn	Si	P	S	Ni
Percent weight	0.10	22.0	1.50	9.00	0.60	18.50	1.00	1.00	0.04	0.03	bal.

the sense that after the imposition of a variety of relaxation and cyclic tests, a few loading cycles returned the specimen back to the same response for any particular type of loading. It was therefore possible to run a variety of strain histories on a single specimen. To verify that the sample did not change state during the tests, the response of the sample to an intermediate strain rate cycle of simple tension was checked after a certain test sequence to ensure that no long term state changes were occurring.

Tests were conducted at three different strain rates, *viz.* 10^{-3}, 10^{-4} and 10^{-5} s^{-1} for tension–compression, pure torsion, in-phase tension–torsion, as well as out-of-phase tension–torsion loadings. It is noteworthy that at 982°C almost no additional cyclic hardening occurred due to nonproportional straining as has often been observed in other materials (Lamba and Sidebottom, 1978; McDowell, 1985). Tests were conducted in which relaxation strain holds were imposed at various strain points around a steady-state hysteresis loop executed at a constant strain rate. In addition, tests in which the strain rate was suddenly changed by a factor of 10 or 20 were conducted. These tests provide a broad test of the predictive capabilities of the proposed self-consistent model and specific results will be presented later in the paper.

3. COORDINATE SYSTEMS

In order to describe the proposed model, it is necessary to designate three coordinate systems and their associated unit basis vectors. The coordinate systems used are shown in Fig. 1. In general, it is convenient to locate a coordinate system such that one axis coincides with the specimen axis. This coordinate system will be referred to as the global coordinate system and has axes x, y, z with unit vectors $\mathbf{i}, \mathbf{j}, \mathbf{k}$. It is also convenient to locate the crystallographic coordinate system with axes aligned along the edges of a unit cell in the FCC structure. This coordinate system will be referred to as the x^*, y^*, z^* system with unit vectors $\mathbf{i}^*, \mathbf{j}^*, \mathbf{k}^*$. Finally, convenient coordinate systems in which to describe the constitutive behavior of individual slip systems are those with one axis on the slip plane in the slip direction whose associated unit vector is $\mathbf{m}$, with a second axis normal to the slip plane whose associated unit vector is denoted by $\mathbf{n}$, and a third axis in the slip plane, normal to the slip direction, having an associated unit vector $\mathbf{z} = \mathbf{m} \times \mathbf{n}$. The stress tensor in the global system x, y, z will be denoted by σ_{ij} and the stress tensor in the crystallographic system x^*, y^*, z^* by σ^*_{ij}. If Q_{ij} denotes the orthogonal tensor which rotates the crystallographic (starred) axes into the global (unstarred) axes, *viz.* $x_i = Q_{ij}x^*_j$, then the stress and strain rate tensors in the crystallographic system may be obtained from the stress and strain rate tensors in the global system from the usual transformation relations

$$\sigma^*_{ij} = Q_{ki}\sigma_{kl}Q_{lj} \quad \text{and} \quad (\dot{\varepsilon}^{T*}_{ij}, \dot{\varepsilon}^{P*}_{ij}) = Q_{ki}(\dot{\varepsilon}^{T}_{kl}, \dot{\varepsilon}^{P}_{kl})Q_{lj}, \tag{1}$$

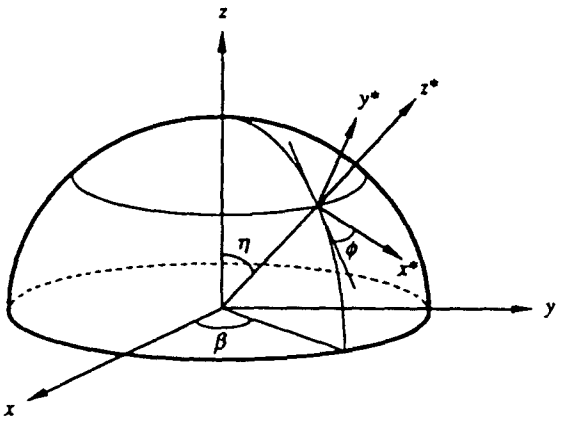

Fig. 1. Relation between the global axes x, y, z and the crystallographic axes x^*, y^*, z^*.

where the matrix Q_{ij} is given, in terms of the appropriate Euler angles in Fig. 1, by

$$(Q_{ij}) = \begin{bmatrix} \cos\eta\cos\beta\cos\phi - \sin\beta\sin\phi & -\cos\eta\cos\beta\sin\phi - \sin\beta\cos\phi & \sin\eta\cos\beta \\ \cos\eta\sin\beta\cos\phi + \cos\beta\sin\phi & -\cos\eta\sin\beta\sin\phi + \cos\beta\cos\phi & \sin\eta\sin\beta \\ -\sin\eta\cos\phi & \sin\eta\sin\phi & \cos\eta \end{bmatrix}. \tag{2}$$

and the superscripts T and P on $\dot{\varepsilon}_{ij}$ denote the total and plastic components, respectively.

4. THE SINGLE CRYSTAL CONSTITUTIVE FORMULATION

The rate-dependent constitutive behavior of the single crystal is represented by a unified viscoplastic formulation based on crystallographic slip theory. This viscoplastic single crystal relation for Hastelloy-X at elevated temperature has been recently developed by Jordan *et al.* (1992) and is a modification of the model developed by Walker and Jordan (1985, 1992). A basic assumption of the formulation is that the component of stress responsible for the shear deformation on a given slip system is the resolved shear stress on the slip plane and in the slip direction. The behavior of the single crystal is derived from a viscoplastic constitutive relation which is assumed to give the slip behavior of each individual slip system. In this formulation, creep and plastic strains are represented as a single inelastic strain (hence the term unified) and the effects of deformation history are accounted for by state variables that evolve according to their own differential evolution equations. The formulation, as applied to each Schmid shear stress component in the octahedral slip system, is summarized by the following equations:

$$\pi_r^o = \mathbf{m}_r^o \cdot \boldsymbol{\sigma}^* \cdot \mathbf{n}_r^o, \quad r = 1, 2, \ldots, 12, \tag{3}$$

$$\dot{\gamma}_r^o = \left| \frac{\pi_r^o - \omega_r^o}{K_r^o} \right|^{n-1} \left(\frac{\pi_r^o - \omega_r^o}{K_r^o} \right), \quad r = 1, 2, \ldots, 12, \tag{4}$$

$$\dot{\omega}_r^o = \varrho_1^o \dot{\gamma}_r^o - \varrho_2^o |\dot{\gamma}_r^o| \omega_r^o - \varrho_3^o |\omega_r^o|^{p-1} \omega_r^o, \quad r = 1, 2, \ldots, 12, \tag{5}$$

$$\dot{K}_r^o = \sum_{k=1}^{12} \{\beta_1 [q_1 + (1-q_1)\delta_{rk}] - \beta_2 [q_2 + (1-q_2)\delta_{rk}](K_r^o - K_1^o)\} |\dot{\gamma}_k^o|, \quad r = 1, 2, \ldots, 12, \tag{6}$$

where n, p, ϱ_1^o, ϱ_2^o, ϱ_3^o, β_1, β_2, q_1, q_2, K_1^o are temperature dependent octahedral material constants with K_1^o being the initial value of each slip system drag stress; π_r^o is the Schmid stress on the octahedral plane of the rth system; $\dot{\gamma}_r^o$ is the shear strain rate due to slip on the rth octahedral slip system; ω_r^o, K_r^o are the octahedral back stress and drag stress state variables in the rth octahedral slip system; and δ_{rk} is the Kronecker delta tensor. The constants q_1 and q_2 are connected with latent hardening interaction effects between the slip systems in which slip on intersecting systems influences the behavior on the slip systems of interest. The formulation for cube slip systems is represented in an analogous manner except the drag stress is assumed to be constant. The equations for cube slip are given as follows:

$$\pi_r^c = \mathbf{m}_r^c \cdot \boldsymbol{\sigma}^* \cdot \mathbf{n}_r^c, \quad r = 1, 2, \ldots, 6, \tag{7}$$

$$\dot{\gamma}_r^c = \left| \frac{\pi_r^c - \omega_r^c}{K_r^c} \right|^{m-1} \left(\frac{\pi_r^c - \omega_r^c}{K_r^c} \right), \quad r = 1, 2, \ldots, 6, \tag{8}$$

$$\dot{\omega}_r^c = \varrho_1^c \dot{\gamma}_r^c - \varrho_2^c |\dot{\gamma}_r^c| \omega_r^c - \varrho_3^c |\omega_r^c|^{q-1} \omega_r^c, \quad r = 1, 2, \ldots, 6, \tag{9}$$

$$K_r^c = K_1^c, \quad r = 1, 2, \ldots, 6, \tag{10}$$

Table 2.

Octahedral vectors		
$\mathbf{m}_1^o = (\mathbf{i}^* - \mathbf{k}^*)/\sqrt{2}$	$\mathbf{n}_1^o = (\mathbf{i}^* + \mathbf{j}^* + \mathbf{k}^*)/\sqrt{3}$	$\mathbf{z}_1^o = (\mathbf{i}^* - 2\mathbf{j}^* + \mathbf{k}^*)/\sqrt{6}$
$\mathbf{m}_2^o = (-\mathbf{i}^* + \mathbf{j}^*)/\sqrt{2}$	$\mathbf{n}_2^o = (\mathbf{i}^* + \mathbf{j}^* + \mathbf{k}^*)/\sqrt{3}$	$\mathbf{z}_2^o = (\mathbf{i}^* + \mathbf{j}^* - 2\mathbf{k}^*)/\sqrt{6}$
$\mathbf{m}_3^o = (-\mathbf{j}^* + \mathbf{k}^*)/\sqrt{2}$	$\mathbf{n}_3^o = (\mathbf{i}^* + \mathbf{j}^* + \mathbf{k}^*)/\sqrt{3}$	$\mathbf{z}_3^o = (-2\mathbf{i}^* + \mathbf{j}^* + \mathbf{k}^*)/\sqrt{6}$
$\mathbf{m}_4^o = (\mathbf{j}^* - \mathbf{k}^*)/\sqrt{2}$	$\mathbf{n}_4^o = (-\mathbf{i}^* + \mathbf{j}^* + \mathbf{k}^*)/\sqrt{3}$	$\mathbf{z}_4^o = (2\mathbf{i}^* + \mathbf{j}^* + \mathbf{k}^*)/\sqrt{6}$
$\mathbf{m}_5^o = (-\mathbf{i}^* - \mathbf{j}^*)/\sqrt{2}$	$\mathbf{n}_5^o = (-\mathbf{i}^* + \mathbf{j}^* + \mathbf{k}^*)/\sqrt{3}$	$\mathbf{z}_5^o = (-\mathbf{i}^* + \mathbf{j}^* - 2\mathbf{k}^*)/\sqrt{6}$
$\mathbf{m}_6^o = (\mathbf{i}^* + \mathbf{k}^*)/\sqrt{2}$	$\mathbf{n}_6^o = (-\mathbf{i}^* + \mathbf{j}^* + \mathbf{k}^*)/\sqrt{3}$	$\mathbf{z}_6^o = (-\mathbf{i}^* - 2\mathbf{j}^* + \mathbf{k}^*)/\sqrt{6}$
$\mathbf{m}_7^o = (-\mathbf{i}^* - \mathbf{k}^*)/\sqrt{2}$	$\mathbf{n}_7^o = (-\mathbf{i}^* - \mathbf{j}^* + \mathbf{k}^*)/\sqrt{3}$	$\mathbf{z}_7^o = (-\mathbf{i}^* + 2\mathbf{j}^* + \mathbf{k}^*)/\sqrt{6}$
$\mathbf{m}_8^o = (\mathbf{i}^* - \mathbf{j}^*)/\sqrt{2}$	$\mathbf{n}_8^o = (-\mathbf{i}^* - \mathbf{j}^* + \mathbf{k}^*)/\sqrt{3}$	$\mathbf{z}_8^o = (-\mathbf{i}^* - \mathbf{j}^* - 2\mathbf{k}^*)/\sqrt{6}$
$\mathbf{m}_9^o = (\mathbf{j}^* + \mathbf{k}^*)/\sqrt{2}$	$\mathbf{n}_9^o = (-\mathbf{i}^* - \mathbf{j}^* + \mathbf{k}^*)/\sqrt{3}$	$\mathbf{z}_9^o = (2\mathbf{i}^* - \mathbf{j}^* + \mathbf{k}^*)/\sqrt{6}$
$\mathbf{m}_{10}^o = (-\mathbf{j}^* - \mathbf{k}^*)/\sqrt{2}$	$\mathbf{n}_{10}^o = (\mathbf{i}^* - \mathbf{j}^* + \mathbf{k}^*)/\sqrt{3}$	$\mathbf{z}_{10}^o = (-2\mathbf{i}^* - \mathbf{j}^* + \mathbf{k}^*)/\sqrt{6}$
$\mathbf{m}_{11}^o = (\mathbf{i}^* + \mathbf{j}^*)/\sqrt{2}$	$\mathbf{n}_{11}^o = (\mathbf{i}^* - \mathbf{j}^* + \mathbf{k}^*)/\sqrt{3}$	$\mathbf{z}_{11}^o = (\mathbf{i}^* + \mathbf{j}^* - 2\mathbf{k}^*)/\sqrt{6}$
$\mathbf{m}_{12}^o = (-\mathbf{i}^* + \mathbf{k}^*)/\sqrt{2}$	$\mathbf{n}_{12}^o = (\mathbf{i}^* - \mathbf{j}^* + \mathbf{k}^*)/\sqrt{3}$	$\mathbf{z}_{12}^o = (\mathbf{i}^* + 2\mathbf{j}^* + \mathbf{k}^*)/\sqrt{6}$

where m, q, ϱ_1^c, ϱ_2^c, ϱ_3^c, K_1^c are temperature dependent cube material constants; π_r^c is the Schmid stress on the cube shear plane of the rth system; γ_r^c is the shear strain rate due to slip on the rth cube slip system; and ω_r^c is the back stress state variable in the rth cube slip system. The vectors $\mathbf{m}^o$, $\mathbf{n}^o$, $\mathbf{m}^c$ and $\mathbf{n}^c$ defining the local octahedral and cube slip systems are given in Tables 2 and 3.

In order to make the single crystal constitutive model match the strain rate dependence of both the uniaxial and biaxial single crystal tests, it was found to be necessary to introduce two latent hardening/softening factors, q_1 and q_2. The introduction of the latent softening factor, q_2, into the dynamic recovery terms of the drag stress state variable has not been considered in the literature heretofore, and a detailed discussion is given in Jordan *et al.* (1992).

The basic formulation involving active octahedral slip on close packed planes in close packed directions is accepted as standard for FCC single crystals. The authors were unable to find evidence in the literature, either for or against, for cube slip in Hastelloy-X single crystal specimens. There is, however, evidence for such slip in nickel base gamma prime superalloys (Walker and Jordan, 1985) and the introduction of this assumption allowed good agreement between the single crystal predictions and experiments on Hastelloy-X to be obtained. It is clear from the single crystal predictions in the preceding reference that octahedral slip alone does not give good predictions for single crystal specimens with their axes oriented in the [011] or [$\bar{1}$11] crystallographic directions. Further plastic straining from some other quarter is indicated. This is found to be true at lower temperatures where cube slip is generally acknowledged to be inoperative. Thus, in both the nickel base gamma prime superalloys and the current Hastelloy-X single crystal specimens, additional slip other than octahedral in conjunction with the octahedral slip itself is needed in order to harmonize the calculations with the experimental results. In default of metallurgical evidence, we have assumed that this extra plastic deformation is due to slip on the cube systems in the FCC structure, and we have made the simplest assumption that the drag stress in the cube system is constant and that no interaction occurs between the octahedral and cube slip systems.

Table 3

Cube vectors		
$\mathbf{m}_1^c = (\mathbf{i}^* + \mathbf{j}^*)/\sqrt{2}$	$\mathbf{n}_1^c = \mathbf{k}^*$	$\mathbf{z}_1^c = (\mathbf{i}^* - \mathbf{j}^*)/\sqrt{2}$
$\mathbf{m}_2^c = (-\mathbf{i}^* + \mathbf{j}^*)/\sqrt{2}$	$\mathbf{n}_2^c = \mathbf{k}^*$	$\mathbf{z}_2^c = (\mathbf{i}^* + \mathbf{j}^*)/\sqrt{2}$
$\mathbf{m}_3^c = (\mathbf{i}^* + \mathbf{k}^*)/\sqrt{2}$	$\mathbf{n}_3^c = \mathbf{j}^*$	$\mathbf{z}_3^c = (-\mathbf{i}^* + \mathbf{k}^*)/\sqrt{2}$
$\mathbf{m}_4^c = (-\mathbf{i}^* + \mathbf{k}^*)/\sqrt{2}$	$\mathbf{n}_4^c = \mathbf{j}^*$	$\mathbf{z}_4^c = (-\mathbf{i}^* - \mathbf{k}^*)/\sqrt{2}$
$\mathbf{m}_5^c = (\mathbf{j}^* + \mathbf{k}^*)/\sqrt{2}$	$\mathbf{n}_5^c = \mathbf{i}^*$	$\mathbf{z}_5^c = (\mathbf{j}^* - \mathbf{k}^*)/\sqrt{2}$
$\mathbf{m}_6^c = (-\mathbf{j}^* + \mathbf{k}^*)/\sqrt{2}$	$\mathbf{n}_6^c = \mathbf{i}^*$	$\mathbf{z}_6^c = (\mathbf{j}^* + \mathbf{k}^*)/\sqrt{2}$

5. CRYSTAL DEFORMATION BY SUMMATION OF SLIP ON INDIVIDUAL SLIP SYSTEMS

The overall deformation of the crystal is determined by summing the deformation on the 12 octahedral and six cube slip systems. In summing up the slip from the various slip systems, a knowledge of the slip geometry determined by material scientists is used, in combination with appropriate tensor transformations, to get the overall inelastic strain rate in the crystallographic axes. In each of the 18 *mn* type directions the shear strain rates are governed by the relations described in the preceding section. The inelastic strain rate tensor in each slip system, $(\mathbf{m}_r^\alpha, \mathbf{n}_r^\alpha, \mathbf{z}_r^\alpha)$, where $\alpha = o$ or c, is then of the form

$$\begin{pmatrix} \dot{\varepsilon}^\alpha_{mm} & \dot{\varepsilon}^\alpha_{mn} & \dot{\varepsilon}^\alpha_{mz} \\ \dot{\varepsilon}^\alpha_{nm} & \dot{\varepsilon}^\alpha_{nn} & \dot{\varepsilon}^\alpha_{nz} \\ \dot{\varepsilon}^\alpha_{zm} & \dot{\varepsilon}^\alpha_{zn} & \dot{\varepsilon}^\alpha_{zz} \end{pmatrix} = \begin{pmatrix} 0 & \frac{1}{2}\dot{\gamma}^\alpha_r & 0 \\ \frac{1}{2}\dot{\gamma}^\alpha_r & 0 & 0 \\ 0 & 0 & 0 \end{pmatrix}.$$

These 18 tensors are then rotated into the common crystallographic system $(\mathbf{i}^*, \mathbf{j}^*, \mathbf{k}^*)$ and summed according to the relation,

$$\dot{\varepsilon}^{P^*}_{ij} = \sum_{r=1}^{12} \tfrac{1}{2}[(\mathbf{i}^* \cdot \mathbf{n}_r^o)(\mathbf{m}_r^o \cdot \mathbf{j}^*) + (\mathbf{i}^* \cdot \mathbf{m}_r^o)(\mathbf{n}_r^o \cdot \mathbf{j}^*)]\dot{\gamma}^o_r + \sum_{r=1}^{6} \tfrac{1}{2}[(\mathbf{i}^* \cdot \mathbf{n}_r^c)(\mathbf{m}_r^c \cdot \mathbf{j}^*) + (\mathbf{i}^* \cdot \mathbf{m}_r^c)(\mathbf{n}_r^c \cdot \mathbf{j}^*)]\dot{\gamma}^c_r, \quad (11)$$

to get the overall inelastic strain rate, $\dot{\varepsilon}^{P^*}_{ij}$, of the crystal in the crystallographic axes x^*, y^*, z^*.

The stress rate tensor with respect to the crystallographic axes is then determined from Hooke's law according to the relationship

$$\dot{\sigma}^*_{ij} = D^c_{ijkl}(\dot{\varepsilon}^{T^*}_{kl} - \dot{\varepsilon}^{P^*}_{kl}) + \dot{D}^c_{ijkl}(\varepsilon^{T^*}_{kl} - \varepsilon^{P^*}_{kl}), \quad (12)$$

where D^c_{ijkl} is the anisotropic elasticity tensor for the face-centered cubic crystal referred to the crystallographic axes x^*, y^*, z^*. The stress rate and the strain rates in the global system are then obtained from the inverse of eqn (1), *viz.*

$$\dot{\sigma}_{ij}(\eta, \beta, \phi) = Q_{ik}\dot{\sigma}^*_{kl}Q_{jl} \quad \text{and} \quad (\dot{\varepsilon}^T_{ij}(\eta, \beta, \phi), \dot{\varepsilon}^P_{ij}(\eta, \beta, \phi)) = Q_{ik}(\dot{\varepsilon}^{T^*}_{kl}, \dot{\varepsilon}^{P^*}_{kl})Q_{jl}. \quad (13)$$

The last term in eqn (12) is zero under the isothermal conditions considered in this paper.

6. DETERMINATION OF THE MATERIAL CONSTANTS

The proposed equations governing the single crystal behavior contain material constants that must be determined from experiments on single crystal specimens. Because of the nature of the equations these constants cannot be readily determined from slopes or other attributes of the test data. Constants were determined by means of a Levenberg–Marquardt nonlinear least squares approach (Press *et al.*, 1986) which adjusts the constants to minimize the square of the sum of the stress difference between the experimental data and the model predictions. It is possible to determine the octahedral material constants independently of the cube material constants by using data from [001] uniaxial tension–compression tests, because in [001] tension-compression tests the resolved shear stresses on all the cube planes are zero. The cube material constants may then be determined from [001] torsion data once the octahedral material constants are known. The constants for the octahedral slip system were determined from three [001] steady state tension–compression hysteresis loops having a strain range of $\pm 0.3\%$ and strain rates of 10^{-3}, 10^{-4} and 10^{-5} s^{-1}. Cube slip constants were determined from three [001] steady state pure torsion hysteresis loops having a strain range of $\pm 0.4\%$ and strain rates of 10^{-3}, 10^{-4} and 10^{-5} s^{-1}. The latent hardening constants q_1 and q_2 were determined from three sets of [001] steady state biaxial hysteresis loops in which both the axial and torsional strain range was $\pm 0.4\%$.

Table 4. Material constants for Hastelloy-X single crystal at 982°C [from Jordan *et al.* (1992)]

$\varrho_1^0 = 111.90 \times 10^9$ N m^{-2}	$\varrho_1^c = 5.864 \times 10^9$ N m^{-2}
$\varrho_2^0 = 1.796 \times 10^4$	$\varrho_2^c = 6.093 \times 10^3$
$\varrho_3^0 = 0$ (N m^{-2})$^{-(p-1)}$.s^{-1}	$\varrho_3^c = 0$ (N m^{-2})$^{-(q-1)}$.s^{-1}
$n = 3.995$	$m = 4.780$
$p = 3.0$	$q = 3.0$
$K_1^0 = 2.550 \times 10^8$ N m^{-2}.s^{-n}	$K_1^c = 2.840 \times 10^8$ N m^{-2}.s^{-m}
$\beta_1 = 588.72 \times 10^9$ N m^{-2}.s^{-m}	
$\beta_2 = 4.731 \times 10^4$	$D_{1111}^c = 103.59 \times 10^9$ N m^{-2}
$q_1 = 2.0$	$D_{1122}^c = 58.27 \times 10^9$ N m^{-2}
$q_2 = 0.5$	$D_{1212}^c = 83.08 \times 10^9$ N m^{-2}

The material constants determined for the single crystal version of Hastelloy-X at 982°C are shown in Table 4. After all the model constants were determined from the experimental data, predictions for the single crystal version of Hastelloy-X were made for strain rate sensitivity tests under various biaxial loadings, strain rate dip tests, relaxation tests and out-of-phase biaxial tests. These results, presented in Jordan *et al.* (1992), show that the agreement between the model predictions and the experiments for Hastelloy-X single crystal is very good.

7. SELF-CONSISTENT MODEL

If the individual crystalline grains of the polycrystalline material are assumed to be spherical, then Eshelby's analysis (1957) shows that the stress state inside a single crystal which is immersed in an infinite isotropic matrix is homogeneous. For self-consistency we require that the orientation average of the microscopic constitutive relation over the grain, when constrained by the effective isotropic matrix (i.e. the polycrystal), should correspond to the constitutive relation for the overall effective isotropic medium, i.e.

$$\Delta\sigma_{ij}^0 = \langle D_{ijkl}(\eta,\beta,\phi)(\Delta\varepsilon_{kl}^T(\eta,\beta,\phi) - \Delta\varepsilon_{kl}^P(\eta,\beta,\phi))\rangle = \bar{D}_{ijkl}(\Delta\varepsilon_{kl}^0 - \Delta\bar{\varepsilon}_{kl}^P), \tag{14}$$

where $\Delta\varepsilon_{kl}^0$ is the applied uniform strain increment on the polycrystal; $\Delta\sigma_{ij}^0$ is the effective incremental stress response of the polycrystal; $\bar{D}_{ijkl}$ is the effective isotropic elasticity tensor for the polycrystal; $\Delta\bar{\varepsilon}_{kl}^P$ is the inelastic strain increment in the polycrystal; and (η,β,ϕ) are the Euler angles for the orientation of the crystallographic axes with respect to global axes in the polycrystalline material as shown in Fig. 1. The tensor $D_{ijkl}(\eta,\beta,\phi)$ is the elasticity tensor of the grain; $\Delta\varepsilon_{kl}^T(\eta,\beta,\phi)$ is the total strain increment in the grain; and $\Delta\varepsilon_{kl}^P(\eta,\beta,\phi)$ is the inelastic strain increment in the grain, all referred to the global coordinate system. The orientation averaging is denoted by

$$\langle f(\eta,\beta,\phi)\rangle = \frac{1}{8\pi^2}\int_{\eta=0}^{\pi}\int_{\beta=0}^{2\pi}\int_{\phi=0}^{2\pi} f(\eta,\beta,\phi)\sin\eta\,d\eta\,d\beta\,d\phi. \tag{15}$$

By using an integral equation approach (see the Appendix) the total strain increment in the anisotropic spherical grain, when constrained by the isotropic effective medium (polycrystal), is given in the global coordinate system by the relation

$$\begin{aligned}\Delta\varepsilon_{ij}^T(\eta,\beta,\phi) = {} & [I_{ijmn} + S_{ijef}\bar{D}_{efpq}^{-1}(D_{pqmn}(\eta,\beta,\phi) - \bar{D}_{pqmn})]^{-1} \\ & \times \{\Delta\varepsilon_{mn}^0 + S_{mnkl}(\Delta\varepsilon_{kl}^P(\eta,\beta,\phi) - \Delta\bar{\varepsilon}_{kl}^P) + S_{mnkl}\bar{D}_{klrs}^{-1}(D_{rsrs}(\eta,\beta,\phi) - \bar{D}_{rsrs}) \\ & \times \Delta\varepsilon_{rs}^P(\eta,\beta,\phi)\},\end{aligned} \tag{16}$$

in which I_{ijmn} is the fourth rank identity tensor. The Eshelby tensor, S_{ijkl}, for the case of an isotropic effective medium (polycrystal) is given by the relation

$$S_{ijkl} = (1 - \tfrac{5}{3}\beta)\delta_{ij}\delta_{kl} + \tfrac{1}{2}\beta(\delta_{ik}\delta_{jl} + \delta_{il}\delta_{jk} - \tfrac{2}{3}\delta_{ij}\delta_{kl}), \tag{17}$$

where $\beta = 2(4-5\bar{\nu})/[15(1-\bar{\nu})]$ and $\bar{\nu} = \bar{\lambda}/[2(\bar{\lambda}+\bar{\mu})]$ is Poisson's ratio for the effective medium (polycrystal). The isotropic elasticity tensor for the effective medium is given by the relation

$$\bar{D}_{ijkl} = \bar{\lambda}\delta_{ij}\delta_{kl} + 2\bar{\mu}(\delta_{ik}\delta_{jl} + \delta_{il}\delta_{jk}), \tag{18}$$

and the elasticity tensor of the spherical single crystal grain in the global system is given by

$$D_{ijkl}(\eta, \beta, \phi) = Q_{ip}(\eta, \beta, \phi)Q_{jq}(\eta, \beta, \phi)Q_{kr}(\eta, \beta, \phi)Q_{ls}(\eta, \beta, \phi)D^{c}_{pqrs}, \tag{19}$$

where the Q_{ip}s are tabulated in eqn (2) and values of D^{c}_{ijkl} for the face centered cubic crystal are given in Table 4. The stress increment in the grain, when referred to the global coordinate system, is then given by the relation

$$\Delta\sigma_{ij}(\eta, \beta, \phi) = D_{ijkl}(\eta, \beta, \phi)(\Delta\varepsilon^{T}_{kl}(\eta, \beta, \phi) - \Delta\varepsilon^{P}_{kl}(\eta, \beta, \phi)). \tag{20}$$

On introducing (16) into (14) and equating the elastic and inelastic components of the stress increment, we obtain an implicit relation for effective elasticity tensor, $\bar{D}_{ijkl}$, and an

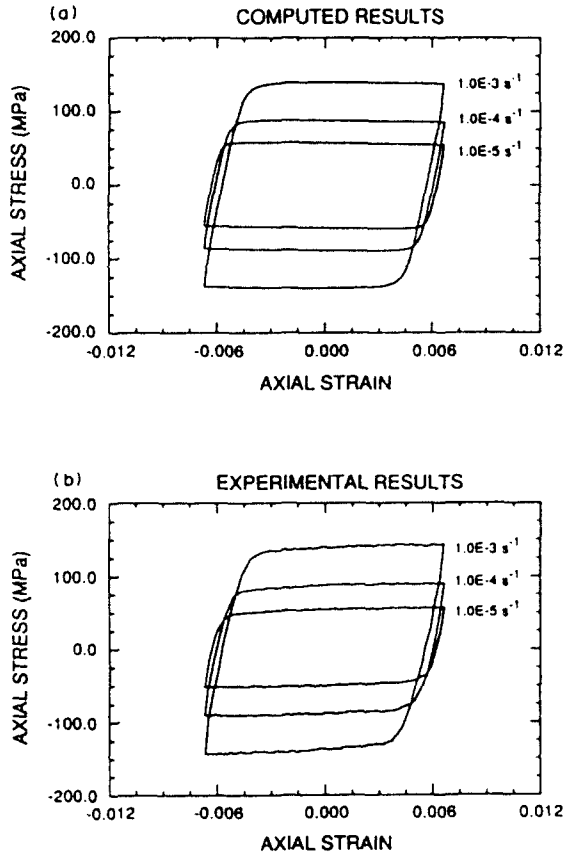

Fig. 2. Hysteresis loops of a uniaxial tension–compression test for polycrystalline Hastelloy-X at 982°C. (a) Prediction of the self-consistent model. (b) Polycrystalline experimental results.

explicit expression for effective inelastic strain increment, $\Delta\bar{\varepsilon}^{p}_{kl}$, *viz.*

$$\bar{D}_{ijkl} = \langle D_{ijrs}(\eta, \beta, \phi)[I_{rskl} + S_{rspq}\bar{D}^{-1}_{pqmn}(D_{mnkl}(\eta, \beta, \phi) - \bar{D}_{mnkl})]^{-1}\rangle \tag{21}$$

and

$$\Delta\bar{\varepsilon}^{p}_{ij} = [\bar{D}_{ijpq}(S_{pqrs} - I_{pqrs})]^{-1}\langle D_{rsuv}(\eta, \beta, \phi)[I_{uvgh} + S_{uvef}\bar{D}^{-1}_{efmn} \times (D_{mngh}(\eta, \beta, \phi) - \bar{D}_{mngh})]^{-1}(S_{ghkl} - I_{ghkl})\Delta\varepsilon^{p}_{kl}(\eta, \beta, \phi)\rangle. \tag{22}$$

The effective elasticity tensor of the polycrystal in eqn (21) may be obtained by iteration at the start of the calculation. Values of $\bar{\lambda} = 40.08 \times 10^{9}$ N m^{-2} and $\bar{\mu} = 49.96 \times 10^{9}$ N m^{-2} for the polycrystal were obtained by iterating (21) with values of D^{c}_{ijkl} given in Table 4, which may be compared with experimental values of $\bar{\lambda}_{expt} = 41.72 \times 10^{9}$ N m^{-2} and $\bar{\mu}_{expt} = 53.16 \times 10^{9}$ N m^{-2}. The overall effective polycrystal constitutive relation in eqn (14) is then easily computed. Suppose that the stress state, $\sigma_{ij}(\eta, \beta, \phi)$, in the grain is known. The inelastic strain increment in the grain, $\Delta\varepsilon^{p}_{kl}(\eta, \beta, \phi)$, can be determined from eqn (11) by integrating the unified viscoplastic slip formulation described in the preceding section with an explicit Euler forward difference method. The corresponding inelastic strain increment in the effective medium of the polycrystal is obtained from eqn (22). The stress increment in the overall effective medium (polycrystal) is then calculated from eqn (14). Equation (20) for the stress increment in the grain, $\Delta\sigma_{ij}(\eta, \beta, \phi)$, is then used to update the stress state in each grain at each set of Euler angles (η, β, ϕ) used in the numerical orientation averaging scheme, in preparation for the next overall integration increment.

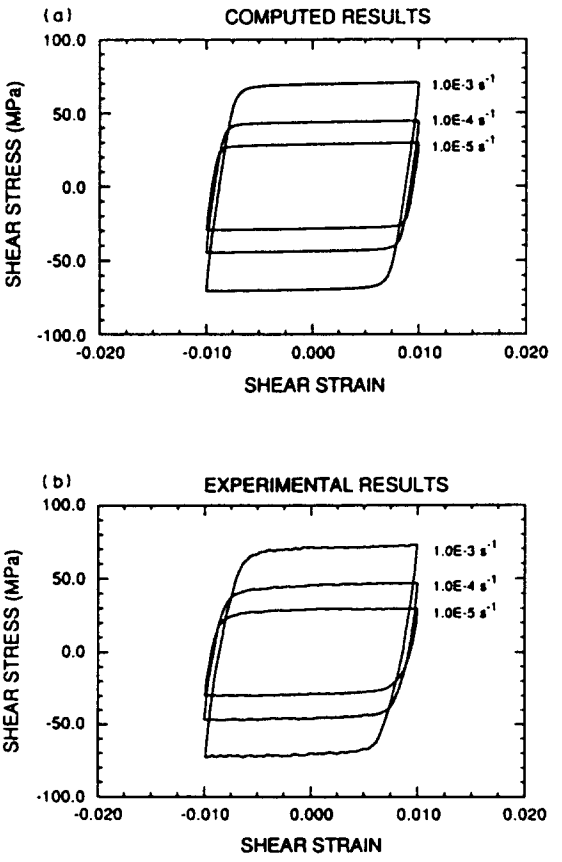

Fig. 3. Hysteresis loops of a pure torsion test for polycrystalline Hastelloy-X at 982°C. (a) Prediction of the self-consistent model. (b) Polycrystalline experimental results.

In the numerical work the orientation averages in eqn (15) were computed with an $8 \times 8 \times 8$ Gaussian quadrature scheme. The accuracy was checked by comparing the results with a more refined $12 \times 12 \times 12$ Gaussian quadrature.

The predicted results from the self-consistent calculations show a very subtle strain softening in the saturated portions of the hysteresis loops, even though the single crystal constitutive model itself shows no softening in the saturated portions of the single crystal hysteresis loops. We have, however, observed softening in the self-consistent calculations any time the isotropic elastic moduli are not exactly self-consistent. For example, the elastic moduli were computed with a $12 \times 12 \times 12$ quadrature scheme at the start of the calculations, whilst the hysteresis loops themselves were computed with an $8 \times 8 \times 8$ quadrature scheme. The slight self-inconsistency thus introduced produces the slight strain softening observed in some of the figures, e.g. (4a, 6a), in the saturated portions of the hysteresis loops.

It should be noted from the Appendix that the method is explicit provided the inelastic strain increment in the grain is independent of the total strain increment in the grain. This requirement is met if the viscoplastic model is integrated by means of an Euler forward difference method, since in this case the inelastic strain increment depends only on the state of the grain at the beginning of the increment. However, if a backward difference or other implicit integration method is used (including forward difference subincrementing), then the inelastic strain increment will depend on the total strain increment, and the integral equation in the Appendix results in an iterative procedure for the determination of the inelastic strain increment in the grain.

8. MODEL PREDICTIONS AND EXPERIMENTAL RESULTS

To verify the self-consistent formulations derived in the preceding section, critical verification experiments were conducted on the polycrystal version of Hastelloy-X and the

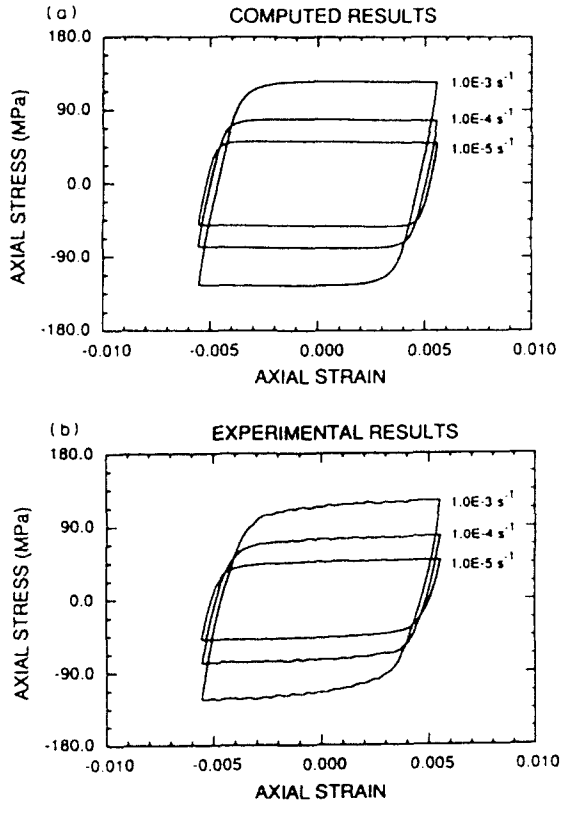

Fig. 4. Axial response of a biaxial test ($\lambda = 1.0$) for polycrystalline Hastelloy-X at 982°C. (a) Prediction of the self-consistent model. (b) Polycrystalline experimental results.

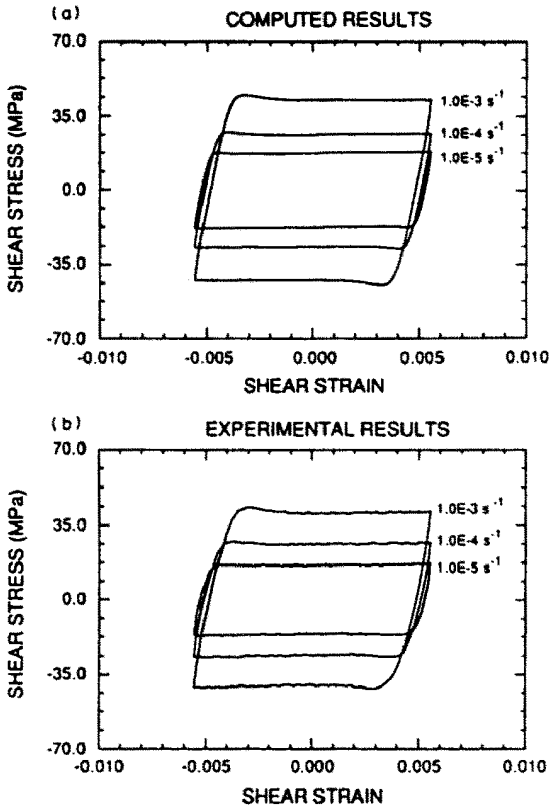

Fig. 5. Torsional response of a biaxial test ($\lambda = 1.0$) for polycrystalline Hastelloy-X at 982°C. (a) Prediction of the self-consistent model. (b) Polycrystalline experimental results.

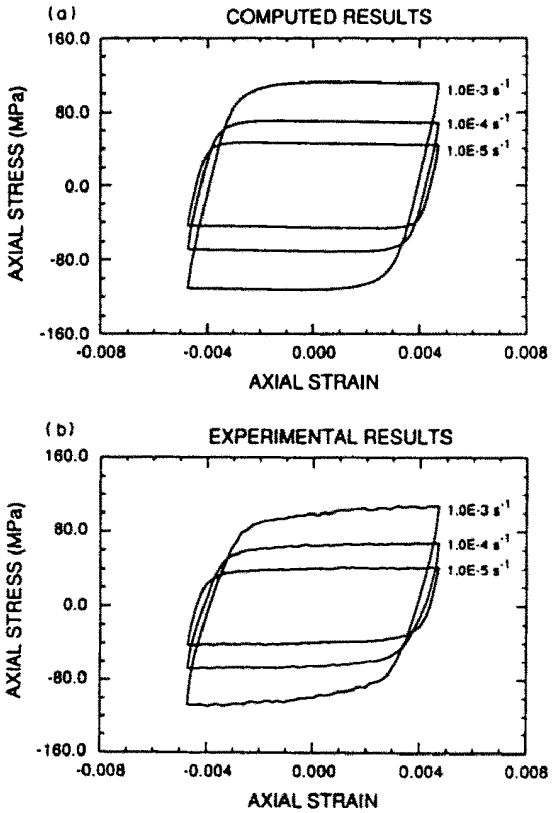

Fig. 6. Axial response of a biaxial test ($\lambda = 1.5$) for polycrystalline Hastelloy-X at 982°C. (a) Prediction of the self-consistent model. (b) Polycrystalline experimental results.

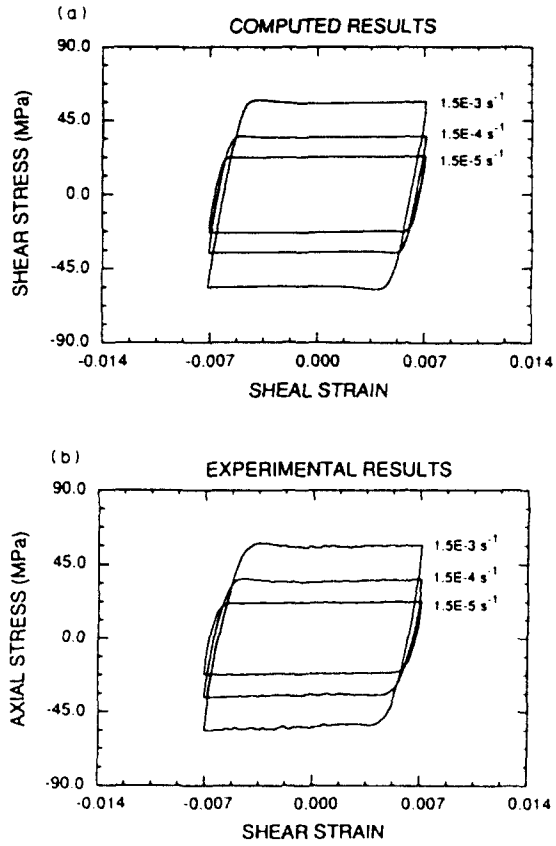

Fig. 7. Torsional response of a biaxial test ($\lambda = 1.5$) for polycrystalline Hastelloy-X at 982°C. (a) Prediction of the self-consistent model. (b) Polycrystalline experimental results.

test results were compared with the model predictions. Figure 2 shows the comparison of model prediction and experimental data under tension–compression cyclic loading with a strain range of $\pm 0.67\%$ and strain rates of 10^{-3}, 10^{-4} and $10^{-5}\ s^{-1}$ at 982°C. Figure 3 shows the comparison of the self-consistent model prediction and experimental data under pure torsional cyclic loading with a strain range of $\pm 1.0\%$ and strain rates of 10^{-3}, 10^{-4} and $10^{-5}\ s^{-1}$ at 982°C.

Comparisons of the model predictions and experimental results under biaxial loading at 982°C are shown in Figs 4–7. In Figs 4 and 5 the ratio of the torsional strain range to

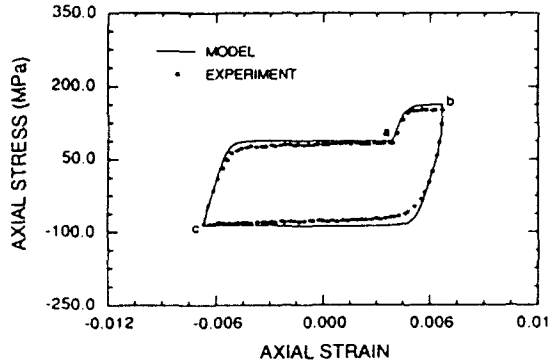

Fig. 8. Comparison of the self-consistent and experimental hysteresis loops of a uniaxial tension–compression strain rate dip test for polycrystalline Hastelloy-X at 982°C with a strain range of $\pm 0.67\%$ under the constant strain rates $2 \times 10^{-3}\ s^{-1}$ from a to b and $1 \times 10^{-4}\ s^{-1}$ from b to c to a.

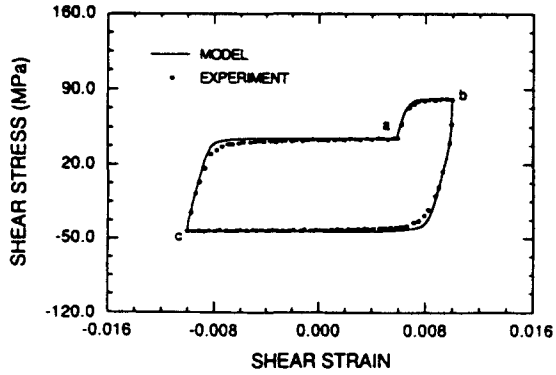

Fig. 9. Comparison of the self-consistent and experimental hysteresis loops of a pure torsional strain rate dip test for polycrystalline Hastelloy-X at 982°C with a strain range of ±1.00% under the constant strain rates $2 \times 10^{-3}\,s^{-1}$ from a to b and $1 \times 10^{-4}\,s^{-1}$ from b to c to a.

the axial strain range, λ, is equal to one, whilst $\lambda = 1.5$ for the biaxial loading in Figs 6 and 7. It is noted that in torsion both the predictions and the experiments indicate a stress overshoot which diminishes with decreasing strain rate.

Figure 8 shows the comparison of the model prediction and experimental result in a uniaxial tension–compression strain rate dip test at 982°C in which the strain rate suddenly increases by a factor of 20 for part of the cycle which was conducted with a strain range of ±0.67%. Figure 9 shows the comparison in a pure torsion strain rate dip test with a strain rate ratio of 20 run at 982°C under a strain range of ±1.0%. The comparison for the relaxation tests conducted at two points on the loading and unloading branches of steady state hysteresis loops are shown in Figs 10 and 11.

The predicted macroscopic response of the polycrystal has been calculated directly from the single crystal model using the self-consistent method without any adjustable parameters and fits the experimental data very well.

9. SUMMARY

A self-consistent model for polycrystal Hastelloy-X has been developed which uses a unified viscoplastic constitutive single crystal formulation of the same material. The most significant aspect of the results presented in this paper is that the experiments necessary to determine the single crystal constants were carried out independently of the polycrystalline verification experiments. As a result, the polycrystal response predictions were made without any adjustable parameters and are true predictions. The excellent agreement between the

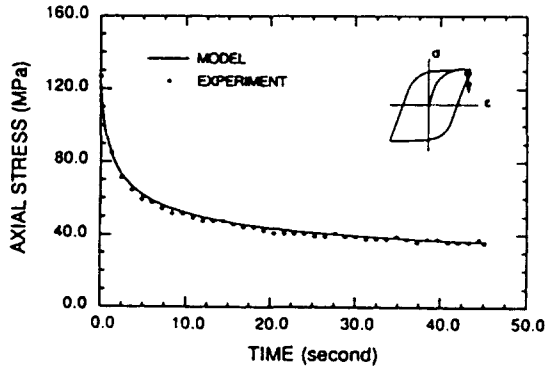

Fig. 10. Stress relaxation behavior of polycrystalline Hastelloy-X at 982°C starting at a strain of 0.655% on the tensile unloading path of a steady state hysteresis loop of a uniaxial tension–compression test with ±0.67% strain range and $1.0 \times 10^{-3}\,s^{-1}$ strain rate.

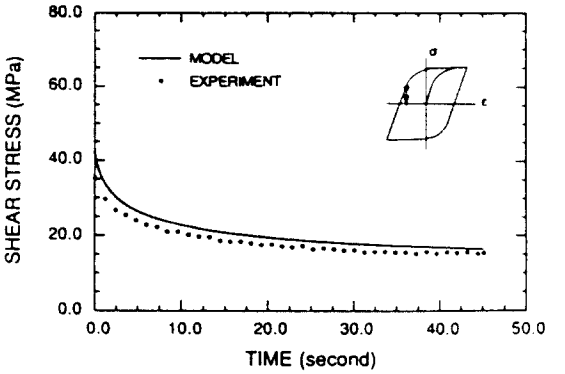

Fig. 11. Stress relaxation behavior of polycrystalline Hastelloy-X at 982 C starting at a strain of −0.783% on the torsional loading path of a steady state hysteresis loop of a pure torsion test with ±1.00% strain range and $1.0 \times 10^{-3}\,s^{-1}$ strain rate.

polycrystalline experiments and the calculations supports the ability of the self-consistent model to predict the overall response of the polycrystalline aggregate for the small strain viscoplastic experiments performed in this study. The present model provides a connection between crystallographic microslip based models of single crystals and polycrystalline metals for the case of coupled viscoplasticity.

The good agreement between the self-consistent calculations and the experimental tests on the polycrystal samples should not be interpreted as applying in all cases. The quality of the agreement would certainly be adversely affected by significant grain boundary sliding. Harmony would also be disrupted if the elastic properties were more anisotropic or if there were less slip systems active and the overall deformation in the crystalline grains were more inhomogeneous.

Acknowledgements—This research was supported by the US Department of Energy under grant DE-FG02-88ER13894 and contract DE-AC02-88ER13895 and also by the NASA Lewis Research Center under grant NAG3-512. Specimens were kindly supplied by Pratt & Whitney.

REFERENCES

Berveiller, M. and Zaoui, A. (1984). Modeling of the plastic behavior of inhomogeneous media. *J. Engng Mater. Tech.* **106**, 295–298.

Bretheau, T., Mussot, P. and Rey, C. (1984). Microscale plastic inhomogeneities and macroscopic behavior of single and multiphase materials. *J. Engng Mater. Tech.* **106**, 304–310.

Chiang, C. R. and Weng, G. J. (1984). Transition of plastic behavior from single crystal to polycrystal under pure tension, and the effect of multislip. *J. Engng Mater. Tech.* **106**, 311–316.

Duva, J. M. (1984). A self-consistent analysis of the stiffening effect of rigid inclusions on a power-law material. *J. Engng Mater. Tech.* **106**, 317–321.

Eshelby, J. D. (1957). The determination of the elastic field of an ellipsoidal inclusion, and related problems. *Proc. R. Soc. Lond.* **A241**, 376–396.

Hutchinson, J. W. (1976). Bounds and self-consistent estimates for creep of polycrystalline materials. *Proc. R. Soc. Lond.* **A348**, 101–127.

Jordan, E. H. and Chan, C. T. (1987). A unique elevated temperature tension-torsion test rig. *Experimental Mechanics* **27**(2), 172–183.

Jordan, E. H., Shi, S. and Walker, K. P. (1992). The viscoplastic behavior of Hastelloy-X single crystal. *Int. J. Plasticity* (in press).

Jordan, E. H. and Walker, K. P. (1992). A viscoplastic model for single crystals. *J. Engng Mater. Tech.* **14**, 19–26.

Kratochvil, J. and Tokuda, M. (1984). Plastic response of polycrystalline metals subjected to complex deformation history. *J. Engng Mater. Tech.* **106**, 299–303.

Lamba, H. S. and Sidebottom, O. M. (1978). Erasure of memory and subsequent strain hardening. *J. Engng Mater. Tech.* **100**, 98–103.

Liu, K. C. (1983). Low-cycle biaxial fatigue of annealed 2 1/4 Cr-1 Mo steel at 538 C under in-phase loads. Oak Ridge National Laboratory Report ORNL-TM-8641, July, 1983.

McDowell, D. L. (1985). A two surface model for transient nonproportional cyclic plasticity: part 1—Development of appropriate equations; part 2—Comparison of theory with experiments. *J. Appl. Mech.* **52**, 298–308.

Nemat-Nasser, S. and Obata, M. (1986). Rate-dependent, finite elasto-plastic deformation of polycrystals. *Proc. R. Soc. Lond.* **A407**, 343–375.

Press, W. H., Flannery, B. P., Teukolsky, S. A. and Vetterling, W. T. (1986). *Numerical Recipes. The Art of Scientific Computing*. Cambridge University Press, UK.

Walker, K. P., Freed, A. D. and Jordan, E. H. (1991). Microstress analysis of periodic composites. *Comp. Engng* 1(1), 29–40.

Walker, K. P. and Jordan, E. H. (1985). Biaxial constitutive modelling and testing of a single crystal superalloy at elevated temperature. In *Biaxial and Multiaxial Fatigue, EGF* 3 (Edited by M. W. Brown and K. J. Miller), pp. 145–170. Mechanical Engineering Publications, London.

Walker, K. P., Jordan, E. H. and Freed, A. D. (1989). Nonlinear mesomechanics of composites witih periodic microstructure: first report. NASA TM 102051.

Walker, K. P., Jordan, E. H. and Freed, A. D. (1990). Equivalence of Green's function and the Fourier series representation of composites with periodic microstructure. In *Micromechanics and Inhomogeneity. The Toshio Mura Anniversary Volume* (Edited by G. J. Weng, M. Taya and H. Abé), pp. 535–558. Springer, Berlin.

APPENDIX

In Walker *et al.* (1989, 1990, 1991) we have shown that the total strain increment $\Delta\varepsilon^{\mathrm{T}}_{kl}(\mathbf{r})$ inside an inclusion (spherical crystal grain) embedded in an "infinite" matrix (polycrystal), upon which a uniform strain increment $\Delta\varepsilon^{0}_{kl}$ is applied at "infinity", is determined by solving the integral equation

$$\Delta\varepsilon^{\mathrm{T}}_{kl}(\mathbf{r}) = \Delta\varepsilon^{0}_{kl} + \int\int\int_{V} U_{klmn}(\mathbf{r}-\mathbf{r}')\{\bar{D}_{mnrs}\Delta\varepsilon^{\mathrm{P}}_{rs}(\mathbf{r}', \Delta\varepsilon^{\mathrm{T}}_{pq}(\mathbf{r}')) - \vartheta(\mathbf{r}')(D_{mnrs}(\mathbf{r}') - \bar{D}_{mnrs}) \times [\Delta\varepsilon^{\mathrm{T}}_{rs}(\mathbf{r}') - \Delta\varepsilon^{\mathrm{P}}_{rs}(\mathbf{r}', \Delta\varepsilon^{\mathrm{T}}_{pq}(\mathbf{r}'))]\}\,\mathrm{d}V(\mathbf{r}'), \quad \text{(A1)}$$

where $\vartheta(\mathbf{r}') = 1$ if $\mathbf{r}'$ is in the inclusion and $\vartheta(\mathbf{r}') = 0$ if $\mathbf{r}'$ is in the matrix. The fourth rank tensor $U_{klmn}(\mathbf{r}-\mathbf{r}')$ gives the kl component of the total strain increment at point $\mathbf{r}$ due to the mn component of a stress increment applied at point $\mathbf{r}'$ in the infinite matrix witih elasticity tensor $\bar{D}_{mnrs}$, i.e.

$$U_{klmn}(\mathbf{r}-\mathbf{r}') = -\frac{1}{2}\left(\frac{\partial^2 G_{km}(\mathbf{r}-\mathbf{r}')}{\partial x_l\,\partial x_n} + \frac{\partial^2 G_{lm}(\mathbf{r}-\mathbf{r}')}{\partial x_k\,\partial x_n}\right). \quad \text{(A2)}$$

The volume integration in eqn (A1) extends over the volume V_{S} of the spherical grain whose elasticity tensor is, in general, given by $D_{mnrs}(\mathbf{r}')$, and over the "infinite matrix" with volume V_{M}.

The Green's function tensor in the "infinite" matrix material is defined by the usual isotropic relation

$$G_{ij}(\mathbf{r}) = \frac{1}{8\pi\bar{\mu}r}\left\{2\delta_{ij} - \frac{\bar{\lambda}+\bar{\mu}}{\bar{\lambda}+2\bar{\mu}}\left(\delta_{ij} - \frac{x_i x_j}{r^2}\right)\right\}, \quad \text{(A3)}$$

where $r = |\mathbf{r}| = \sqrt{x_m x_m}$ is the magnitude of the vector $\mathbf{r}$.

It is known from Eshelby's analysis (1957) that if the initial stress state inside the inclusion is homogeneous, the total strain increment inside the inclusion, $\Delta\varepsilon^{\mathrm{T}}_{kl}(\mathbf{r})$, will also be homogeneous when a uniform strain increment, $\Delta\varepsilon^{0}_{kl}$, is applied to the matrix material. This can readily be seen from (A1), for if we replace $\Delta\varepsilon^{\mathrm{T}}_{rs}(\mathbf{r}')$ inside the integral with a guess of $\Delta\varepsilon^{0}_{kl}$, then the first Rayleigh–Born approximation to the solution of the integral equation is given by

$$\Delta\varepsilon^{\mathrm{T}}_{kl} = \Delta\varepsilon^{0}_{kl} + \int\int\int_{V_{\mathrm{S}}} U_{klmn}(\mathbf{r}-\mathbf{r}')\,\mathrm{d}V(\mathbf{r}')\bar{D}_{mnrs}\Delta\varepsilon^{\mathrm{P}}_{rs}(\Delta\varepsilon^{0}_{pq}) + \int\int\int_{V_{\mathrm{S}}} U_{klmn}(\mathbf{r}-\mathbf{r}')\,\mathrm{d}V(\mathbf{r}')\bar{D}_{mnrs}\Delta\bar{\varepsilon}^{\mathrm{P}}_{rs} - \int\int\int_{V_{\mathrm{S}}} U_{klmn}(\mathbf{r}-\mathbf{r}')\,\mathrm{d}V(\mathbf{r}')\bar{D}_{mnpq}\bar{D}^{-1}_{pquv}(D_{uvrs} - \bar{D}_{uvrs})(\Delta\varepsilon^{0}_{rs} - \Delta\varepsilon^{\mathrm{P}}_{rs}(\Delta\varepsilon^{0}_{rs})). \quad \text{(A4)}$$

We have assumed that $\Delta\varepsilon^{\mathrm{P}}_{kl}(\mathbf{r}') = \Delta\varepsilon^{\mathrm{P}}_{kl}(\Delta\varepsilon^{0}_{pq})$ in the inclusion and that $\Delta\varepsilon^{\mathrm{P}}_{kl}(\mathbf{r}') = \Delta\bar{\varepsilon}^{\mathrm{P}}_{kl}$ in the matrix. In addition, we have also assumed that the inelastic strain increment in the matrix is homogeneous, even in the region immediately outside the inclusion. The strain increments in eqn (A4) have been taken outside the integral because in the Rayleigh–Born approximation they are homogeneous. The volume integral containing the tensor $U_{klmn}(\mathbf{r}-\mathbf{r}')$ is known to be independent of $\mathbf{r}$ if the field point $\mathbf{r}$ lies within the volume V_{S} of the spherical inclusion and hence the first Rayleigh–Born approximation for $\Delta\varepsilon^{\mathrm{T}}_{kl}$ is constant within the inclusion. When this approximate solution for $\Delta\varepsilon^{\mathrm{T}}_{kl}$ is reinserted as a new guess into the integral in eqn (A1), the next and all higher order Rayleigh–Born approximations yield solutions for $\Delta\varepsilon^{\mathrm{T}}_{kl}$ which are homogeneous within the inclusion. This being the case, we may take the strain increments in eqn (A1) outside the integral and write the exact solution to the integral equation as

$$\Delta\varepsilon^{\mathrm{T}}_{kl} = \Delta\varepsilon^{0}_{kl} + S_{klrs}\Delta\varepsilon^{\mathrm{P}}_{rs}(\Delta\varepsilon^{\mathrm{T}}_{uv}) + \int\int\int_{V_{\mathrm{M}}} U_{klmn}(\mathbf{r}-\mathbf{r}')\,\mathrm{d}V(\mathbf{r}')\bar{D}_{mnrs}\Delta\bar{\varepsilon}^{\mathrm{P}}_{rs} - S_{klpq}\bar{D}^{-1}_{pquv}(D_{uvrs} - \bar{D}_{uvrs})(\Delta\varepsilon^{\mathrm{T}}_{rs} - \Delta\varepsilon^{\mathrm{P}}_{rs}(\Delta\varepsilon^{\mathrm{T}}_{uv})), \quad \text{(A5)}$$

where

$$S_{klmn} = \int\int\int_{V_{\mathrm{S}}} U_{klpq}(\mathbf{r}-\mathbf{r}')\,\mathrm{d}V(\mathbf{r}')\bar{D}_{pqmn} \quad \text{(A6)}$$

is Eshelby's tensor which is independent of $\mathbf{r}$ when the field point $\mathbf{r}$ lies in the spherical volume V_S. The volume integral over the matrix can be converted into a surface integral over the surface of the spherical inclusion and over the surface of the matrix at "infinity". Since the field point $\mathbf{r}$ is infinitely removed from the outer surface, the outer surface integral over the matrix vanishes and we are left with the surface integral over the sphere. This can be converted to a volume integral over the sphere and so we find that the volume integral in (A5) can be written as

$$\int\int\int_{V_M} U_{klmn}(\mathbf{r}-\mathbf{r}')\,dV(\mathbf{r}')\bar{D}_{mnrs}\Delta\bar{\varepsilon}^{P}_{rs} = -\int\int\int_{V_S} U_{klmn}(\mathbf{r}-\mathbf{r}')\,dV(\mathbf{r}')\bar{D}_{mnrs}\Delta\bar{\varepsilon}^{P}_{rs} = -S_{klrs}\Delta\bar{\varepsilon}^{P}_{rs}, \tag{A7}$$

in which the minus sign enters because the unit normal over the spherical surface points inwards when the volume integral over the matrix is converted to a surface integral. Equation (A5) may now be solved for $\Delta\varepsilon^{T}_{ij}$ to give

$$\Delta\varepsilon^{T}_{ij}(\eta,\beta,\phi) = [I_{ijmn} + S_{ijef}\bar{D}^{-1}_{efpq}(D_{pqmn}(\eta,\beta,\phi) - \bar{D}_{pqmn})]^{-1} \times \{\Delta\varepsilon^{0}_{mn} + S_{mnkl}(\Delta\varepsilon^{P}_{kl}(\eta,\beta,\phi;\Delta\varepsilon^{T}_{ab}) - \Delta\bar{\varepsilon}^{P}_{kl}) + S_{mnkl}\bar{D}^{-1}_{klwz}(D_{wzrs}(\eta,\beta,\phi) - \bar{D}_{wzrs})\Delta\varepsilon^{P}_{rs}(\eta,\beta,\phi;\Delta\varepsilon^{T}_{ab})\}, \tag{A8}$$

where explicit notice has been taken of the dependence of the spherical grain tensors on the Euler angles (η,β,ϕ) between the crystallographic axes of the grain and the global axes.

When an explicit forward difference method is used to compute the inelastic strain increment in the crystalline grain, the dependence of $\Delta\varepsilon^{P}_{rs}(\eta,\beta,\phi;\Delta\varepsilon^{T}_{ab})$ on $\Delta\varepsilon^{T}_{ab}$ can be dropped and an explicit relation for the total strain increment in the grain is obtained. However, for implicit integration methods, eqn (A8) must be solved iteratively.